Int. J. Electrochem. Sci., 12 **(2017)** 10199 – 10210, doi: 10.20964/2017.11.14

International Journal of
ELECTROCHEMICAL
SCIENCE
www.electrochemsci.org

Effect of the Precipitated Phases on Corrosion Behavior of Mg-Y-Nd Ternary Alloy

Quantong Jiang[1*], *Xia Zhao*[1], *Kui Zhang*[2], *Xinggang Li*[2], *Jie Zhang*[1], *Baorong Hou*[1]

[1] Marine Corrosion and Protection Centre, Institute of Oceanology, Chinese Academy of Sciences, No. 7 Nanhai Road, Qingdao 266071, China)
[2] State Key Lab for Non-ferrous Metals and Process, General Research Institute for Non-ferrous Metals, Beijing 100088, China)
[*]E-mail: jiangquantong@qdio.ac.cn

Received: 10 July 2017 / *Accepted:* 25 August 2017 / *Published:* 12 October 2017

Mg-5Y-xNd alloys (x=0.5, 1.0, 1.5 wt.%) were investigated to reveal the influence of precipitated phase on corrosion resistance. The microstructure, precipitated phases and corrosion behaviors of different samples were analyzed by scanning electron microscope, energy dispersive spectrometer and X-Ray Diffraction. The volume fraction of the Mg_{12}(Y,Nd) phase increased, whereas that of the Mg_3(Y,Nd) phase decreased with increasing Nd-content. The weight loss rate decreased from 10.9584 $mg \cdot cm^{-2} \cdot d^{-1}$ (23.0126 $mm \cdot y^{-1}$) to 6.2184 $mg \cdot cm^{-2} \cdot d^{-1}$ (13.0586 $mm \cdot y^{-1}$). The open circuit potential, potentiodynamic polarization curve, electrochemical impedance spectroscope and scanning kelvin probe confirmed that the corrosion rates of Mg-5Y-xNd alloys follow the order Mg-5Y-0.5Nd > Mg-5Y-1.0Nd > Mg-5Y-1.5Nd. This phenomenon occurred because the Mg_3(Y,Nd) precipitated phase with a face-centered cubic lattice had a more positive potential than the Mg_{12}(Y,Nd) phase with an orthorhombic lattice. Thus, the Mg_3(Y,Nd) precipitated phase acted as the cathode of the electrochemical reaction, and accelerated the corrosion of the Mg matrix more effectively than the Mg_{12}(Y,Nd) phase.

Keywords: Mg-Y-Nd alloy; Microstructure; Precipitated phase; corrosion resistance; Electrochemistry

1. INTRODUCTION

The Mg-Y-Nd alloy system has been successfully applied in the aerospace and automotive industries due to its high strength and creep resistance [1-3]. Yttrium serves as an effective solid solution hardener therefore Y-containing Mg alloys possess good mechanical properties [4-6]. Neodymium can refine the grain size of magnesium alloy and improve the creep resistance of Mg

alloys [7-8]. Many commercial alloys based on the Mg-Y-Nd system have been successfully developed, including WE43, WE54, and EW75 alloys [9-12].

Recently, considerable effort has been devoted to elucidating the influence on corrosion resistance in the Mg-Y-Nd alloy system [13]. Davenport et al. [6] demonstrated that Y-rich regions decelerate the propagation of corrosion, and that the corrosion rate in WE43 alloy is decreased by homogenous Y distribution. Zhang et al. [7] found that grain refinement and fine dispersed $Mg_{12}Nd$ improve the corrosion properties of Mg-Nd-Zn-Zr alloys. Williams et al. [8] analyzed the influence of Nd-content (0.47-3.53 wt.%) on the corrosion properties of Mg alloy and found that the cathodic activation of corroded regions is derived from the Nd-rich intermetallic grains. Zucchi et al. [9] studied the corrosion behavior of WE43 alloy in 3.5% NaCl via electrochemical techniques, and found that the presence of rare earth improves the tendency of Mg to passivation. Nie et al. [10-11] proved that different precipitated phases, such as, Mg_3Nd, Mg_{12}(Y,Nd), Mg_3(Y,Nd), and $Mg_{14}Y_2Nd$ could form in the Mg-Y-Nd alloy system. A literature carefully highlighted the influence on corrosion response of Mg alloy with the addition of Nd, including electrochemical data from precipitation in isolation [12]. However, the influence of Nd-content on the corrosion properties of the Mg-Y-Nd alloy system due to the microstructure and electrochemical activity of the precipitated phases has not been elucidated well. Consequently, studies on this topic are interesting and necessary for scientific research and practical applications.

In this work, Mg-5Y-xNd (x = 0.5, 1.0, 1.5 wt.%) alloys were investigated to reveal the precipitated phases transferred with Nd-content on the corrosion properties. The microstructure, precipitated phases and corrosion behaviors of different samples were studied. The precipitated phases changed from Mg_3(Y,Nd) to continuous Mg_{12}(Y,Nd) with the increasing Nd-content. The Mg_3(Y,Nd) precipitated phase with face-centered cubic lattice had a more positive potential than the Mg_{12}(Y,Nd) phase with orthorhombic lattice, which acted as the cathode of the electrochemical reaction to accelerate the corrosion of Mg matrix more effectively than the Mg_{12}(Y,Nd) phase.

2. EXPERIMENTAL METHODS

2.1. Materials

Table 1. Compositions of different alloys detected by ICP-AES.

Elements / Alloys	Y (wt.%)	Nd (wt.%)	Al (wt.%)	Fe (wt.%)	Cu (wt.%)	Ni (wt.%)
Mg-5Y-0.5Nd	5.00	0.498	0.018	0.024	＜0.01	＜0.01
Mg-5Y-1.0Nd	5.11	1.02	0.027	0.021	＜0.01	＜0.01
Mg-5Y-1.5Nd	5.02	1.50	0.019	0.013	＜0.01	＜0.01

The materials were prepared by melting in an electrical resistance furnace in a steel crucible under protected gas consisting of Ar and $C_2H_2F_4$ to prevent the burning of the melts. The alloys were prepared from blending the appropriate proportions of ingots of commercial purity Mg (>99.95%), Y (99.9%) and Nd (99.9%). The highest smelting temperature was 850 ^oC and the cast temperature was between 720 ^oC and 750 ^oC. The samples were cut from the ingot using an electric spark linear cutting machine. Experimental samples were prepared with nominal levels of Mg-5Y-0.5Nd, Mg-5Y-1.0Nd, and Mg-5Y-1.5Nd alloys. The actual compositions, along with the major impurity levels, were detected by inductively coupled plasma-atomic emission spectroscopy (ICP-AES) (Table 1).

2.2 Electrochemical/corrosion testing

The samples were polished with up to 5000 grit SiC paper, and then measured using three replicate samples for each alloy in 3.5% NaCl solution for 24 h. The corrosion products were removed in boiling chromic acid (20% CrO_3 + 1% $AgNO_3$) for 5 min [13-15].

The open circuit potential (OCP), potentiodynamic polarization curve and electrochemical impedance spectra were obtained from a Solatron 2273 system. Potentiodynamic scanning was performed at 0.5 mV/s after the cell was held at the OCP for 400 s; Electrochemical impedance spectroscopy was conducted at the frequency ranged of 10,000 - 0.1 Hz with 5 mV of sinusoidal potential signals with respect to the OCP.

2.3 Analysis and characterization

The microstructure of the different samples was characterized by scanning electron microscopy (SEM). X-ray diffraction (XRD) analysis was conducted on the alloys to confirm the phase identification with CuKα radiation at 40 kV and 40 mA. A scanning kelvin probe (SKP) was used to acquire information about the local nobility of different microstructures and phases at the submicron scale [16]. The working probe step was 10 μm, scanning in the central location (length = 500 μm, width = 500 μm) of the Mg-5Y-1.5Nd sample. The measurement was taken at room temperature in the atmosphere.

After the immersion test, the samples were quickly washed with deionized water, dried and then weighed to obtain their final weight (W_1). The difference between W_0 and W_1 is the corrosion weight loss (Δw) [17]. The surface morphologies of the different samples without corrosion products were observed by SEM.

3. RESULTS AND DISCUSSION

3.1 Microstructure of Mg-5Y-xNd alloys

Fig. 1 shows the microstructure of Mg-5Y-xNd alloys, which mainly consisted of the primary α and precipitated phases. The average grain sizes of the different alloys were similar, which implied that

grain size did not influence the corrosion rates of the different samples. Precipitated phases were distributed along the grain boundaries of the Mg-5Y-xNd alloys, and were discretely dispersed with a modest volume fraction. The precipitated phases acted as the cathode of the electrochemical reactions to accelerate corrosion [18]. The eutectic precipitated phases formed a continuous uniform distribution with increasing Nd-content.

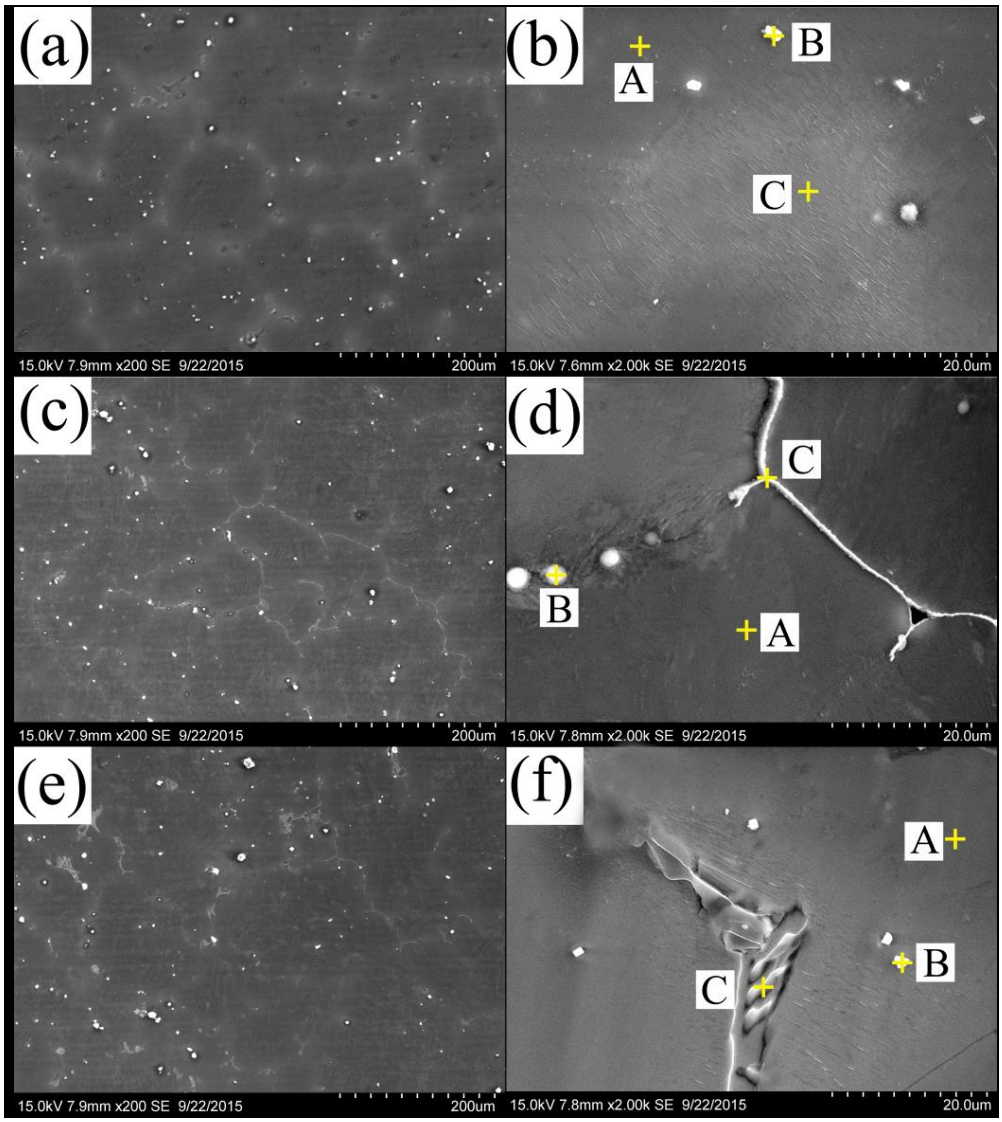

Figure 1. SEM micrographs results of the different alloys: (a) Mg-5Y-0.5Nd magnified 200 times, (b) Mg-5Y-0.5Nd magnified 2000 times with EDS spots, (c) Mg-5Y-1.0Nd magnified 200 times, (d) Mg-5Y-1.0Nd magnified 2000 times with EDS spots, (e) Mg-5Y-1.5Nd magnified 200 times, (f) Mg-5Y-1.5Nd magnified 2000 times with EDS spots.

The EDS results of the individual precipitated phases (Fig.1) of the different samples are shown in Table 2. The gray matrix location ("A") mainly contained Mg, and few Y and Nd element existed. The white contrast particle phases (are labeled "B") and the eutectic phases (are labeled "C"). The difference between "B" and "C" was that the Y element in "B" was higher than in "C", while the Nd element demonstrated the opposite characteristic. According to the results, spot "B" was arranged to be

$Mg_3(Y,Nd)$, while spot "C" was considered to be $Mg_{12}(Y,Nd)$, which was consistent with the research of Nie [10-11]. The contents of Y and Nd in B and C were larger than that of the Mg matrix (A) due to enrichment of the solute atoms in the solid/liquid interface during non-equilibrium solidification [19-20].

Table 2. EDS results of the different alloys in Figure 1.

Position	Alloys	Mg (at.%)	Y (at.%)	Nd (at.%)	Results
A	Mg-5Y-0.5Nd	99.050	0.917	0.032	
	Mg-5Y-1.0Nd	99.236	0.624	0.140	α-Mg
	Mg-5Y-1.5Nd	99.377	0.533	0.090	
B	Mg-5Y-0.5Nd	73.288	26.480	0.232	
	Mg-5Y-1.0Nd	74.621	25.108	0.271	$Mg_3(Y,Nd)$
	Mg-5Y-1.5Nd	74.051	25.745	0.204	
C	Mg-5Y-0.5Nd	91.908	5.512	2.580	
	Mg-5Y-1.0Nd	92.023	5.471	2.505	$Mg_{12}(Y,Nd)$
	Mg-5Y-1.5Nd	91.936	5.226	2.838	

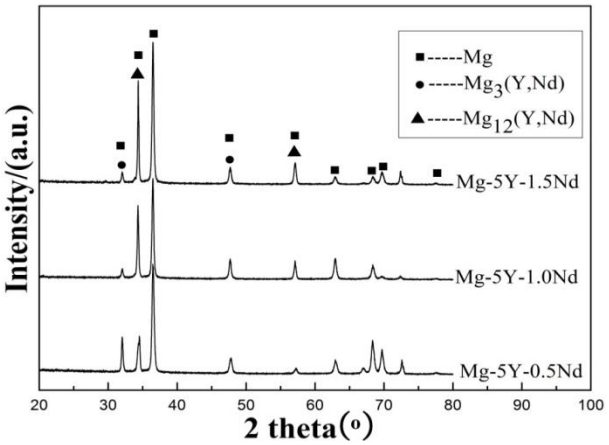

Figure 2. XRD analysis of Mg-5Y-xNd alloys (x = 0.5, 1.0, 1.5 wt.%).

The XRD results of the Mg-5Y-xNd alloys are shown in Fig. 2, which indicated that the Mg diffraction peak was obvious. Moreover, the $Mg_3(Y,Nd)$ (FCC a = 0.74, V = 0.405224 nm^3) and $Mg_{12}(Y,Nd)$ (orthorhombic a = 0.64 nm, b = 2.24 nm, c = 0.52 nm, V = 0.645472 nm^3) precipitated phases were present in the Mg-5Y-xNd alloys. However, the characteristic peak intensity of $Mg_{12}(Y,Nd)$ increased with the Nd-content, whereas that of $Mg_3(Y,Nd)$ was decreased. In previous studies, the $Mg_{12}(Y,Nd)$ and $Mg_3(Y,Nd)$ precipitated phases were both the common eutectic phases in Mg-Y-Nd alloys, but the coexistence of the two eutectic phases coexisting in the grain boundary was rarely observed [21-23].

3.2 Weight loss rates and surface morphologies

The corrosion rate was calculated as follows: $\Delta W = (W_0 - W_1)/S$, where C is the weight loss due to corrosion (mg·cm^{-2}), W_0 is the original weight (mg), W_1 is the final weight without corrosion products (mg), and S is the surface area (cm^2). Three samples of each type were employed, and corrosion rate was the average value. This measurement of the corrosion rate is an average measurement over the immersion time, and an average over the entire samples area. The corrosion rate P_W (mm·y^{-1}) was determined from as follows [24-25]:

$$P_W = 2.10\ \Delta W \quad (1)$$

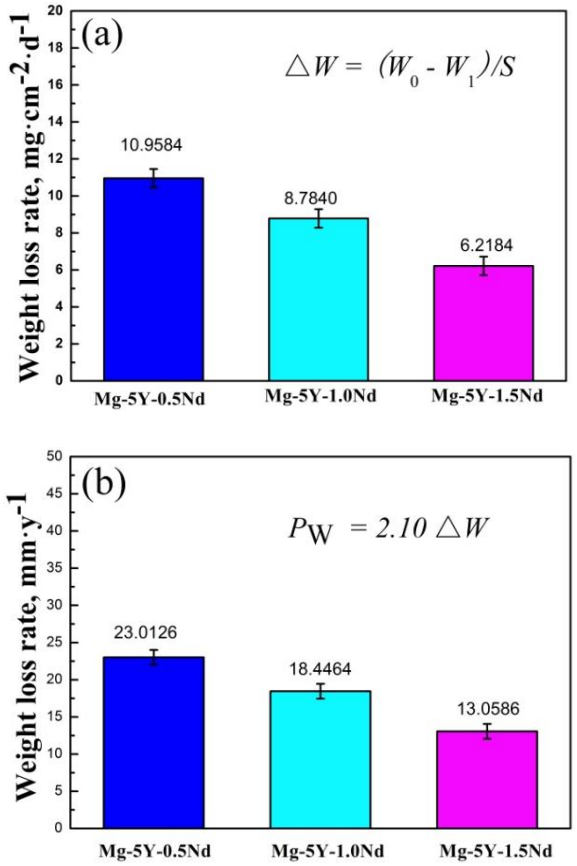

Figure 3. Weight loss rates (mg·cm^{-2}·d^{-1} and mm·y^{-1}) of the different samples.

The Mg-5Y-0.5Nd alloy showed the highest corrosion rate of 10.9584 mg·cm^{-2}·d^{-1} (23.0126 mm·y^{-1}), whereas the Mg-5Y-1.5Nd alloy was showed the opposite at 6.2184 mg·cm^{-2}·d^{-1} (13.0586 mm·y^{-1}), which indicate that the corrosion rates of the different alloys decreased with increasing Nd-content. The weight loss rates follow the order Mg-5Y-0.5Nd＜Mg-5Y-1.0Nd＜Mg-5Y-1.5Nd.

The samples were immersed in 3.5% NaCl solution for 24 h. Then the corrosion products were removed in boiling chromic acid. The surface morphologies without corrosion products are shown in Fig. 4. The corrosion attack of the Mg-5Y-0.5Nd alloy occurred seriously as shown Fig. 4(a), while the bright the precipitated phases remained on the surface of the sample. The uncorroded matrix and precipitated phases were irregularly distributed on the surface of Mg-5Y-1.0Nd alloy as shown Fig.

4(b), whereas the skeleton eutectic phases remained on the surface of the Mg-5Y-1.5Nd alloy in Fig. 4(c). This phenomenon also confirmed that the type and distribution of the precipitated phases determined the corrosion rates of the different alloys.

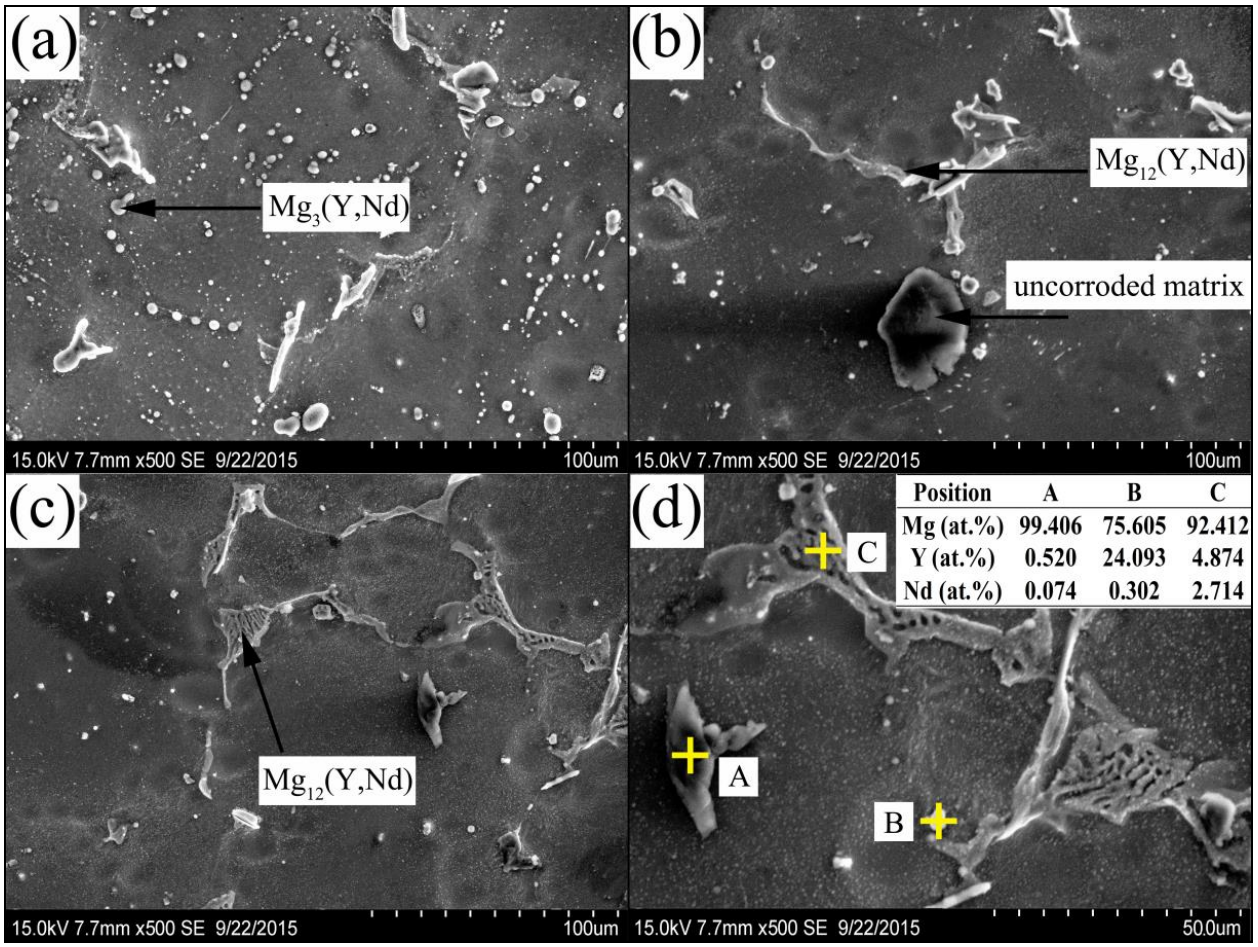

Figure 4. Surface morphologies of the different alloys without corrosion products magnified 500 times: (a) Mg-5Y-0.5Nd; (b) Mg-5Y-1.0Nd; (c) Mg-5Y-1.5Nd (d) Mg-5Y-1.5Nd with EDS spots.

3.3 Electrochemical characterization and analysis

The electrochemical tests of the different alloys measured in 3.5% NaCl solution with the corrosion potential (E_{corr}) and corrosion current (I_{corr}) are shown in Fig. 5. The OCP was comparatively stable before the measurement; in addition, a corrosion product film formed on the surface of the samples, and no clear localized corrosion occurred [26-27]. The Mg-5Y-1.5Nd alloy had the most positive OCP among the alloys, which implied that the electrochemically activity of the Mg-5Y-1.5Nd alloy was the lowest. In the Tafel extrapolation method for measuring the Mg corrosion rate, the corrosion current density, I_{corr} (mA/cm^2) is estimated by the Tafel extrapolation of the cathodic branch of the polarization curve, and I_{corr} is related to the average corrosion rate using [28]:

$$P_i = 22.85\, I_{corr} \qquad (2)$$

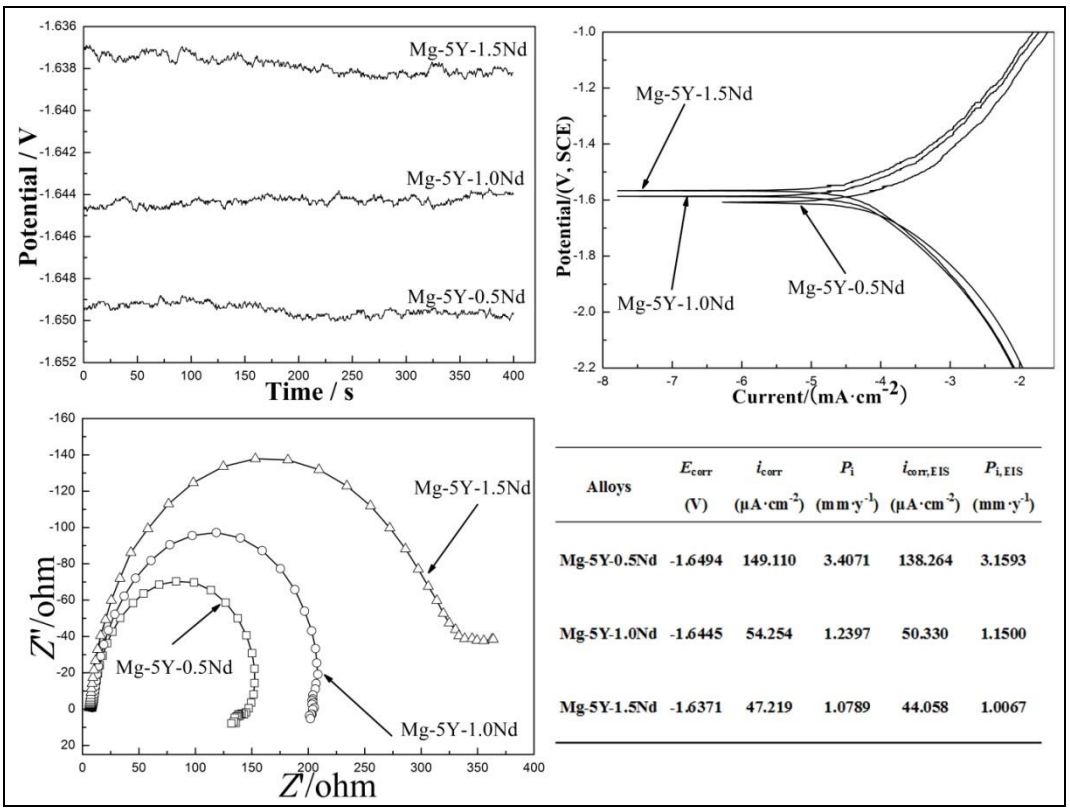

Alloys	E_{corr} (V)	i_{corr} (μA·cm^{-2})	P_i (mm·y^{-1})	$i_{corr,EIS}$ (μA·cm^{-2})	$P_{i,EIS}$ (mm·y^{-1})
Mg-5Y-0.5Nd	-1.6494	149.110	3.4071	138.264	3.1593
Mg-5Y-1.0Nd	-1.6445	54.254	1.2397	50.330	1.1500
Mg-5Y-1.5Nd	-1.6371	47.219	1.0789	44.058	1.0067

Figure 5. Electrochemical test results of the different alloys measured in 3.5% NaCl solution with the corrosion potential (E_{corr}) and corrosion current (I_{corr}).

The I_{corr} values of the Mg-5Y-xNd alloy (x=0.5, 1.0, 1.5 wt.%) were 149.110, 54.254 and 47.219 μA·cm^{-2}, respectively. This phenomenon indicated that the electrochemical corrosion rates of the different alloys follow the order Mg-5Y-0.5Nd＞Mg-5Y-1.0Nd＞Mg-5Y-1.5Nd.

The EIS values of the different alloys also proved this tendency. The corrosion current density, I_{corr} / *EIS* (mA·cm^{-2}) was derived from the polarization resistance, R_P (Ω·cm^{-2}) through the following equation [29]:

$$i_{corr}/\,EIS = \frac{\beta_c\beta_a}{2.3R_p(\beta_c-\beta_a)} = \frac{B}{R_p} \qquad (3)$$

where β_a is the anodic Tafel slope, β_c is the cathodic Tafel slope of the appropriate polarization curve, and B is a constant involving the Tafel slopes as indicated in Eq. The Tafel slopes should be measured from an *iR*-compensated polarization curve, where i is the current density, and R is the resistance between the sample and the measuring reference electrodes. From the polarization resistance, R_P, the corrosion current density, i_{corr} can be evaluated using the following [29-30]:

$$P_{i,\,EIS} = 22.85\, i_{corr}/\,EIS \qquad (4)$$

The Mg-5Y-1.5Nd alloy had the largest EIS value, which illustrated that hydrogen evolution reaction was the most difficult on the α-Mg matrix [31-33]. The average grain sizes of different alloys were similar, indicating that grain size did no tinfluence the corrosion rate. Thus, the type and distribution of the prepicipated phases played an important role in the electrochemical corrosion reaction.

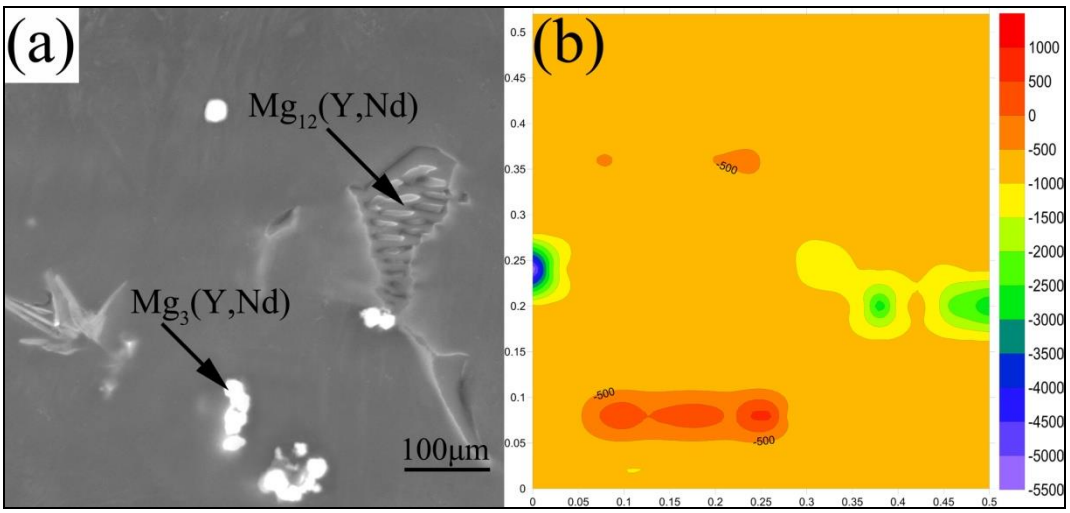

Figure 6. The comparison between SEM photograph (a) and SKP maps (b) obtained from Mg-5Y-1.5Nd alloy.

SKP, which is a non-destructive procedure for measuring the surface distribution of the Volta potential, was developed to investigate the corrosion processes under atmospheric weathering conditions on a micro-scale [34-35]. Fig. 6 shows the comparison between the SEM photograph and the SKP potential maps obtained of the Mg-5Y-1.5Nd alloy. The volta potentials of the Mg_3(Y,Nd) phases, Mg_{12}(Y,Nd) phases and α-Mg matrix were comparable with those recorded by the SEM photograph. As shown in Fig. 6(b), the volta potentials follow the order Mg_3(Y,Nd)＞Mg_{12}(Y,Nd)＞α-Mg matrix. This phenomenon implied that the Mg_3(Y,Nd) and Mg_{12}(Y,Nd) phases served as the cathode of the electrochemical reaction to accelerate the corrosion of the α-Mg matrix. However, the Mg_{12}(Y,Nd) phase as the cathode showed a smaller driving force than Mg_3(Y,Nd) to accelerate the corrosion reaction. Thus, the amount and distribution of Mg_{12}(Y,Nd) phases increased with Nd-content, which decreased the corrosion of α-Mg matrix. That was why that Mg-5Y-1.5Nd alloy had the lowest electrochemically activity and corrosion current density among the alloys.

3.4 Mechanisms of between precipitated phases and corrosion

Fig. 6 shows the Mg_3(Y,Nd) phase, Mg_{12}(Y,Nd) phase and α-Mg matrix of the Mg-5Y-1.5Nd alloy via the SKP technique. Results showed that the Mg_3(Y,Nd) phase of the Mg-5Y-1.5Nd alloy had a more noble potential than the α-Mg matrix, whereas the Mg_{12}(Y,Nd) phase had a smaller potential difference relative to the α-Mg matrix. Thus, the Mg_{12}(Y,Nd) phases had smaller driving force to accelerate corrosion, which played a role in protecting the α-Mg matrix. Therefore, the Mg-5Y-1.5Nd alloy showed the best corrosion resistance.

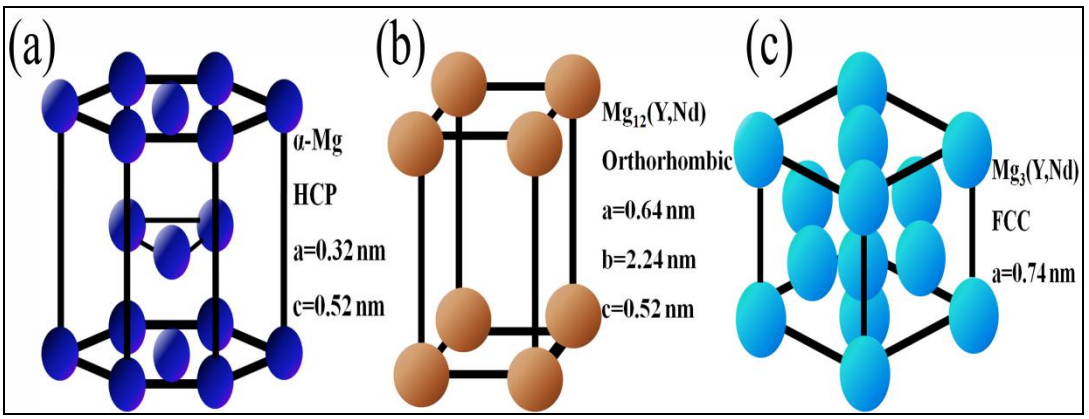

Figure 7. Schematic of the Mg matrix (HCP), $Mg_3(Y,Nd)$ phase (FCC) and $Mg_{12}(Y,Nd)$ phase (Orthorhombic) unit cells.

The $Mg_3(Y,Nd)$ and $Mg_{12}(Y,Nd)$ phases are common precipitated phases in the Mg-Y-Nd ternary alloy system. The crystal structure of the $Mg_3(Y,Nd)$ phase is a FCC lattice, whereas that of $Mg_{12}(Y,Nd)$ phases is an orthorhombic lattice [11]. Fig. 7 shows the schematic of the hexagonal close packed (Mg), face-centered cubic ($Mg_3(Y,Nd)$) and orthorhombic lattices ($Mg_{12}(Y,Nd)$). According to the structure principles of crystalline materials, the density of the FCC lattice is larger than that of the orthorhombic lattice [36]. The larger lattice density signified that the FCC lattice ($Mg_3(Y,Nd)$) was more stable than the orthorhombic lattice ($Mg_{12}(Y,Nd)$), which indicated that $Mg_3(Y,Nd)$ had a lower electrochemical activity than $Mg_{12}(Y,Nd)$ [37-38]. Thus, the $Mg_3(Y,Nd)$ phase has a more positive potential than the $Mg_{12}(Y,Nd)$ phase.

The $Mg_3(Y,Nd)$ and $Mg_{12}(Y,Nd)$ phases were used as the cathode of the electrochemical reaction to accelerate corrosion. In other words, the two precipitated phases have a more positive volta potential than the Mg matrix. Therefore, the potentials of the different phases follow the order Mg $<$ $Mg_{12}(Y,Nd)$ $<$ $Mg_3(Y,Nd)$. The increase of the $Mg_{12}(Y,Nd)$ phase and the decrease of the $Mg_3(Y,Nd)$ phase resulted in the best corrosion resistance of Mg-5Y-1.5Nd. This clearly indicates that the microstructure and the precipitated phase played important roles in corrosion resistance. Moreover, the corrosion resistance of the Mg-Y-Nd alloy can be improved by modifying the type and distribution of precipitated phases.

4. CONCLUSION

(1) Mg-5Y-xNd alloys were investigated to reveal the influence of Nd on anti-corrosion performance. The microstructure of different alloys mainly consisted of the α-Mg matrix, the $Mg_3(Y,Nd)$ phase, and the $Mg_{12}(Y,Nd)$ phase. The amount and volume fraction of the $Mg_{12}(Y,Nd)$ phase increased with the addition of Nd-content, whereas those of the $Mg_3(Y,Nd)$ phase decreased.

(2) The weight loss rate decreased from 10.9584 $mg \cdot cm^{-2} \cdot d^{-1}$ (23.0126 $mm \cdot y^{-1}$) to 6.2184 $mg \cdot cm^{-2} \cdot d^{-1}$ (13.0586 $mm \cdot y^{-1}$) with increasing Nd-content. The electrochemical tests showed a similar

tendency. The corrosion rates of the Mg-5Y-xNd alloys follow the order Mg-5Y-0.5Nd＞Mg-5Y-1.0Nd＞Mg-5Y-1.5Nd.

(3) The type and distribution of precipitated phases of Mg-5Y-xNd alloys played an important role in the corrosion resistance. The Mg_3(Y,Nd) precipitated phase with FCC lattice had a more positive potential than the Mg_{12}(Y,Nd) phase with an orthorhombic lattice, which acted as the cathode of the electrochemical reaction to accelerate the corrosion of Mg matrix more effectively than the Mg_{12}(Y,Nd) phase. Thus, the corrosion resistance of the Mg-Y-Nd alloy could be improved by modifying the precipitated phases.

ACKNOWLEDGEMENTS
The authors gratefully acknowledge the National Natural Science Foundation of China (Grant No. 51501181), the Fundamental Research Project of Technology Program of Qingdao (17-1-1-76-JCH), the Key Research and Development Program of Shandong Province for providing support for this work.

References

1. L.L. Rokhlin, Mg Alloys Containing Rare Earth Metals, (2000) *Taylor and Francis, London, England.*
2. S.Q. Liang, D.K. Guan and X.P Tan, *Mater. Des.*, 32 (2011)1194.
3. J. Wang, J. Meng, D.P. Zhang and D.X. Tang, *Mater. Sci.*, Eng. A. 456 (2007) 78.
4. M. Liu, P. Schmutz, J. Peter, G.L. S and A. Andrej, *Corros. Sci.*, 52 (2010) 3687.
5. J.W. Chang, X.W. Guo, S.M. He, P.H. Fu, L.M. Peng and W.J. Ding, *Corros. Sci.*, 50 (2008) 166.
6. A.D. Sudholz, K. Gusieva, X.B. Chen, B.C. Muddle, M.A. Gibson and N. Birbilis, *Corros. Sci.*, 53 (2011) 2277.
7. N. Birbilis, M.A. Easton, A.D. Sudholz, S.M. Zhu and M.A. Gibson, *Corros. Sci.*, 51 (2009) 683.
8. R.L. Xin, B. Song, K. Zeng, G.J. Huang and Q. Liu, *Mater. Des.*, 34 (2012) 384.
9. F. Zucchi, V. Grassi, A. Frignani, C. Monticelli and G.J. Trabanelli. *Appl. Electrochem*., 36 (2006) 195.
10. J.F. Nie, *Metall. Mater. Trans. A.*, 43 (2012) 3891.
11. J.F. Nie and B.C. Muddle, *Acta. Materialia.*, 48 (2000)1691.
12. V. Neubert, I. Stul´ıkov´, B. Smola, B.L. Mordike, M. Vlach, A. Bakkar and J. Pelcov´a, *Mater. Sci. Eng. A.*, 462 (2007) 329.
13. Q.T. Jiang, K. Zhang, X.G. Li, Y.J. Li, M.L. Ma, G.L. Shi, and J.W. Yuan, *J. Magn. Alloy.*, 1 (2013) 230.
14. Q.T. Jiang, K. Zhang, X.G. Li, Y.J. Li, M.L. Ma, G.L. Shi, and J.W. Yuan, *Corros. Eng. Sci. Techn.*, 49 (2014) 651.
15. M. Esmaily, N. Mortazavi, M. Shahabi-Navid, J.E. Svensson, M. Halvarsson, L. Nyborg, M. Wess´en, E.W. Jarfors and L.G. Johansson, *J. Electrochem. Soc.*, 162 (2015) C85.
16. S. Pawar, X. Zhou, G.E. Thompson, G. Scamans and Z. Fan, *J. Electrochem. Soc.*, 162 (2015) C442.
17. N.D. Nam, *J. Electrochem. Soc.*, 163 (2016) C76.
18. G.L. Song and Z.Q. Xu, *Electrochim. Acta.*, 55 (2010) 4148.
19. R.L. Xin, L. Li, K. Zeng, B. Song and Q. Liu, *Mater. Charact.*, 62 (2011) 535.
20. G. Williams, K. Gusieva, and N. Birbilis, *Corros.*, 68(2012), 489.
21. S.M. Zhu and J.F. Nie, *Scripta. Mater.*, 50 (2004) 51.

22. M.L. Ma, K. Zhang, X.G. Li, Y.J. Li, G.L. Shi and J.W. Yuan, *Mater. Des.*, 51 (2013) 73.
23. M. Li, K. Zhang, X.G. Li, Y.J. Li, M.L. Ma, G.L. Shi, J.W. Yuan, T. Li and J.B. Liu, *Mater. Sci. Eng. A.*, 626 (2015) 415.
24. M.C Zhao, M. Liu, G.L. Song and A. Andrej, *Corros. Sci.*, 50 (2008) 1939.
25. Z.Z. Qiao, Z.M. Shi, H. Norbert, Z.A. Ishida and A. Andrej, *Corros. Sci.*, 61 (2012) 185.
26. G.L. Song and Z.Q. Xu, *Corros. Sci.*, 63 (2012) 100.
27. Z.P. Cano, J.R. McDermid and J.R. Kish, *J. Electrochem. Soc.*, 162 (2015) C732.
28. Z.M. Shi, M. Liu and A. Andrej, Corros. Sci. 52 (2010) 579.
29. Z.M. Shi, F.Y. Cao, G.L. Song and A. Andrej, *Corros. Sci.*, 88 (2014) 434.
30. F.Y. Cao, Z.M. Shi, H. Joelle, J.U. Peter, G.L. Song, M. Liu and A. Andrej, *Corros. Sci.*, 75 (2013) 78.
31. S.Q. Yuan, H. Lu, Z.G. Sun, L. Fan, X.Y. Zhu and W. Zhang, *J. Electrochem. Soc.*, 163 (2016) A1181.
32. W.R. Francis, D.M. Bryan and C.L. Alan, *J. Electrochem. Soc.*, 163 (2016) A958.
33. J.H. Liu, Y.W. Song, J.C. Chen, P. Chen, D.Y. Shan and E.H. Han, *Electrochimica. Acta.*, 190 (2016) 189.
34. Z.P. Cano, J.R. Kish and J.R. Mcdermid, *J. Electrochem. Soc.*, 163 (2016) C62.
35. H. Koji, O.Masayoshi, Y. Michiaki and N. Takayoshi, *Corros. Sci.*, 109 (2016) 68.
36. W.M. Mao, Structure Principles of Crystalline Materials, (2007) *Metallurgical Industry Press, Beijing, China.*
37. J. Bockris and P.K. Subramanyan, *Corros. Sci.*, 10 (1970) 435.
38. N.D. Tomashov, *Corros.*, 20 (1964) 7t.